In situ observation of fracture sequence of physical vapor deposited TiN film on (11$\bar{2}$0) sapphire

Young-Gu Kim and Do Kyung Kim[a)]
Department of Materials Science and Engineering, Korea Advanced Institute of Science and Technology (KAIST), Yusong, Taejon 305-701, Korea

(Received 26 October 2004; accepted 25 March 2005)

The critical parameters for the structural stability of physical vapor deposited TiN film on (11$\bar{2}$0) sapphire were investigated by analyzing the adhesion strength and failure mechanism through in situ observations of the fracture sequence during scratch tests and static normal indentation. TiN was deposited by arc ion plating on (11$\bar{2}$0) sapphire, and the thickness of the TiN film was controlled to 700 nm. Delamination of TiN film was monitored in situ from below the contact through a transparent sapphire substrate, using zoom optics mounted into a video imaging sensor. In situ observation enables us to detect the failure origin of TiN coating on sapphire. The failure origin of TiN film on (11$\bar{2}$0) sapphire was identified as both rhombohedral and basal twinning of the sapphire substrate. Rhombohedral twinning was initiated first, and basal twinning ensued. Twinning-induced plastic deformation of the sapphire substrate triggered the initiation of interfacial delamination of the TiN coating. The plastic deformation of the substrate ultimately induced failure of the protective coating.

I. INTRODUCTION

TiN has excellent properties such as good wear resistance, high corrosion resistance, low friction coefficient, high conductivity, and a bright, golden color. Because of these properties, TiN has been widely used in protective and functional coatings on cutting tools, bearings, etc. To improve the performance of the TiN coating, however, better adhesion between TiN and the substrate is essential. Therefore, evaluation of the mechanical stability of TiN coating on a substrate is critical for obtaining the optimum performance of TiN film.

TiN coating on metallic substrates for the application of cutting tools and diffusion barriers in semiconductor devices has been extensively investigated.[1–6] However, delamination of TiN film leads to premature failure of coatings that are intended to be long lasting. The critical factors that induce failure of TiN coating have not been clearly identified yet. The opaque properties of both TiN film and metallic substrates make it difficult to detect a failure origin occurring at the interfacial region of the coating and substrate. In this respect, due to the transparency of a sapphire substrate, TiN-coated sapphire is potentially an appropriate model structure to observe fracturing of the interfacial region between TiN film and sapphire substrate. TiN-coated sapphire enables observation of the initiation and propagation of failure of TiN film. Furthermore, TiN film coated sapphire has recently seen technological application as electrodes in microelectronic devices because of its high electrical conductivity and low contact resistivity.[7,8]

The purpose of this research is to investigate the critical parameters for structural stability of TiN film on sapphire. In situ observation of the fracture sequence enables us to detect the failure source at the subsurface region.[9] The failure mechanism of TiN film could thus be suggested through in situ observations of the fracture sequence of TiN coated sapphire during scratch tests and static normal indentations.

Sapphire of the (11$\bar{2}$0) plane was prepared as a substrate for TiN film deposition. The surface of the sapphire was polished to 1 μm finish and the roughness of the sapphire surface was then measured by a surface profiler. A surface roughness of R_a = 0.003 μm was obtained. TiN was deposited by cathodic arc ion plating. The substrate holder was heated to 440 °C and Ti ion cleaning continued for 10 min. Working pressure was maintained at 7.3×10^{-3} Torr during deposition. The processing parameters for TiN deposition are summarized in Table I. The substrate holder was rotated at 5 rpm for uniform TiN coating. In a preliminary study, deposition conditions such as bias voltage, N_2 pressure,

a)Address all correspondence to this author.
e-mail: dkkim@kaist.ac.kr
DOI: 10.1557/JMR.2005.0201

TABLE I. Processing parameters during ion plating for TiN deposition.

Parameters	Details
Basic chamber pressure (Torr)	6.0×10^{-6}
Working pressure (Torr)	7.3×10^{-3}
Substrate temperature (°C)	440
Bias voltage (V)	−100
Current (A)	4.6
Deposition time (min)	100
Deposition rate (nm/min)	7
Flowing rate of N_2 (sccm)	95

and substrate temperature were optimized from the standpoint of the TiN phase and uniform TiN composition through TiN. The thickness of the TiN film was linearly proportional to the deposition time. The thickness of TiN film was linearly proportional to the deposition time. The thickness of the TiN film was controlled at 700 nm by fixing the deposition time for 100 min. The phase and structure of TiN were analyzed by x-ray diffraction (XRD) and scanning electron microscopy (SEM) cross-sectional images, respectively. In situ observation equipment was prepared for observing the fracture sequence of TiN coated sapphire during scratch tests and static normal indentations. Figure 1(a) provides a schematic illustration of the in situ observation equipment. The delamination of TiN film was monitored in situ from below the contact through a transparent sapphire substrate, using zoom optics mounted into a video imaging device. Scratch tests (CSEM, CSEM Inc., Swiss) were conducted on the TiN-coated sapphire using a diamond cone indenter with a radius of $r = 200$ μm. The specimens were moved laterally at 10 mm/min for the scratch test. A normal load was applied up to 30 N at 100 N/min. To compare the failure mode of TiN-coated sapphire obtained from the scratch tests, sets of static normal indentations were introduced. During loading and unloading, the fracture sequence was recorded on video tape. After the scratch tests and static indentations, the surface of the TiN coated sapphire was observed by optical microscopy with top and bottom views.

The characteristics of TiN were investigated in the context of TiN phase, orientation, thickness, structure, elastic modulus, and hardness. The TiN thickness was linearly proportional to the deposition time. Deposition rate was maintained at 7 nm/min and TiN phase was analyzed by XRD θ-2θ scan, shown in Fig. 1(b). The peak at 38° was diffracted from the (11$\bar{2}$0) sapphire substrate and peaks of 36°, 42°, and 77° were from (111), (200), and (222) of TiN film, respectively. The preferred growth of TiN to [111] on (11$\bar{2}$0) sapphire was confirmed. The thickness of TiN film was measured from the SEM micrograph showing a cross-sectional view of TiN coated sapphire in Fig. 1(c). TiN film was clearly distinguished from the sapphire substrate. The thickness of TiN was 700 nm and TiN showed a very uniform

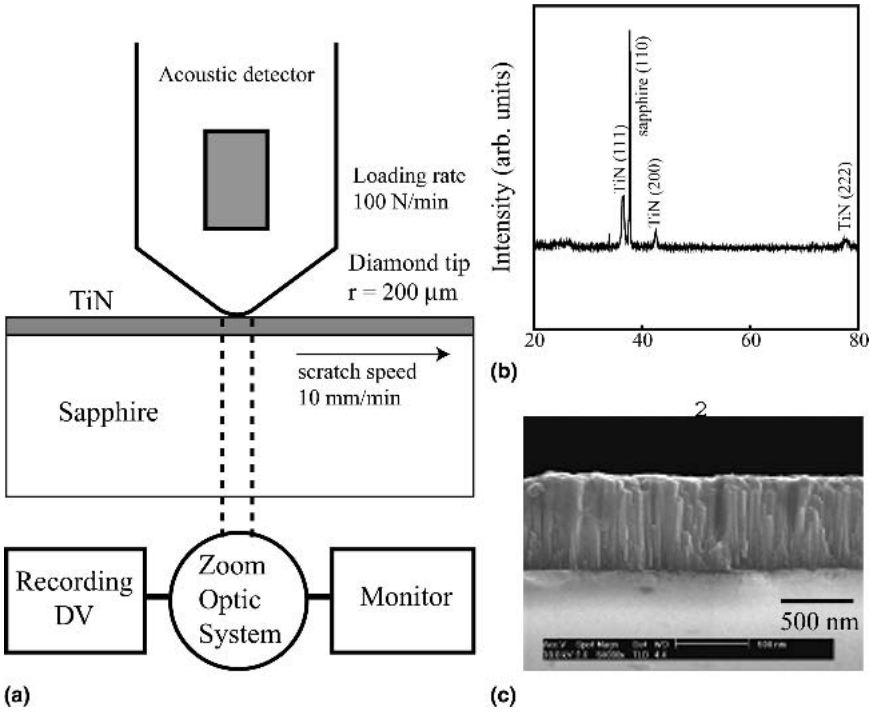

FIG. 1. (a) Schematic illustration of the in-situ observation equipment. (b) XRD pattern showing physical vapor deposition TiN film on (11$\bar{2}$0) sapphire. TiN showed preferred orientation of growth direction to [111]. (c) SEM micrograph showing cross-sectional view of TiN coated sapphire. TiN shows uniform columnar structure and the thickness of TiN was approximately 700 nm.

columnar structure. The column width was about 50 ± 5 nm. The mechanical properties of TiN film were estimated by nano indentation (Triboscope, Hysitron Inc., Minneapolis, MN) with a Berkovich tip of 100 nm curvatures. The maximum load was applied up to 10 mN. At the maximum load, the penetration depth of a Berkovich tip was 130 nm which is less than the one fifth of TiN film. The mechanical properties of TiN film seem to be slightly affected by the substrate considering that the stiffness of sapphire substrate and the penetration depth of one fifth of TiN film.[10] The hardness and elastic modulus of TiN film based on the results of Oliver and Pharr[11] were 26.2 ± 1.4 and 560 ± 5.4 GPa, respectively.

Figure 2 shows a sequence of video clips during a scratch test of 700-nm-thick TiN film on sapphire using a diamond cone indenter with a tip radius of 200 μm. In situ observation of the fracture sequence enables us to detect the initiation and propagation of cracking at the subsurface region. The dark circle indicates the contact area of the diamond indenter on the specimen surface and the numbers displayed on the top left corner denote the normal load. The specimen was moved from right to left. From Figs. 2(a)–2(d), the direction of scratch was conducted along to the direction of [1$\bar{1}$00] . A few linear defects including a faceted defect consisting of two different linear defects appeared at 18.7 N, as shown in Fig. 2(a). Linear defects then formed consecutively, as indicated in Figs. 2(b) and 2(c). Finally, the specimen reached delamination of the TiN film at 20.1 N in Fig. 2(d). Those linear defects were demonstrated, not as some forms of cracking, but as crystal defects of the sapphire substrate. More detailed explanation will be followed in latter parts. The linear defects are clearly visible on sapphire substrate in the part of TiN film peeled off, as shown in Fig. 2(d). The linear features seemed to be on the surface of sapphire substrate and they always

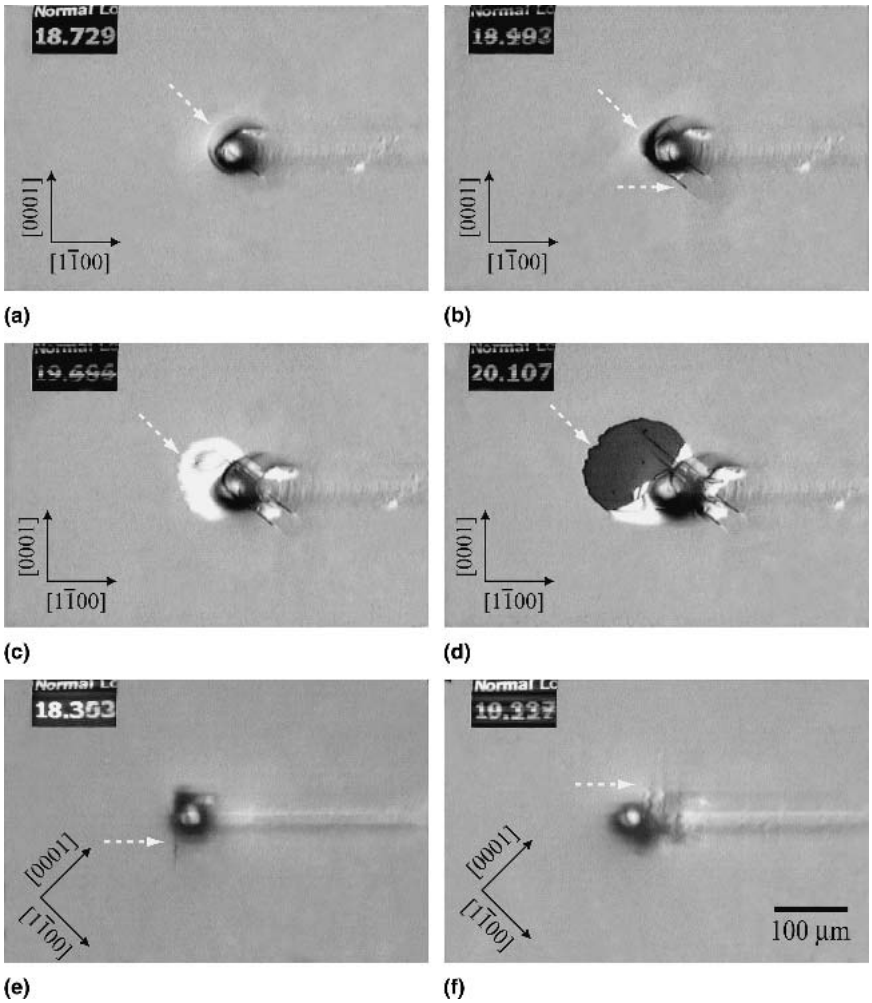

FIG. 2. Sequence of video clips during a scratch test of 700-nm-thick TiN film on sapphire using a diamond cone indenter with a tip radius of 200 μm. The dark circle indicates the contact area of the diamond indenter on the specimen surface and the numbers displayed on the top left corner denote the normal load. The specimen was moved from right to left. (a–d) The direction of scratch was conducted along to the direction of [1$\bar{1}$00] and scratch direction was 45° rotated to the previous direction in (e) and (f).

appeared prior to the delamination of TiN film. The linear defects seem to be highly correlated with the failure of TiN film. The defects in the scratch wake were seemed to be caused by plastic deformation due to the local stress increase near surface defects of TiN film. However, those kinds of defects stayed stable within the scratch channel and did not propagate outwardly.

The scratch direction was 45° rotated to the previous direction in Figs. 2(e) and 2(f). Linear defects were produced perpendicular to the scratch direction. This implies the linear defects were formed with same crystallographic orientation and were independent of the scratch direction.

Sets of static indentation with diamond cone indenter using a tip radius of 200 μm were conducted on the same TiN-coated sapphire for comparison with the scratch tests. The load was applied up to 30 N at 100 N/min, held for 10 s, and then unloaded.

The fracture sequence during static indentation is shown in Fig. 3. It is characterized by four steps. As the normal load increases, the contact area increases, as shown in Fig. 3(a). The first linear defect is initiated at 13.6 N in Fig. 3(b), and it is very similar to the defect that appeared in the former scratch test. Another linear defect at the other side is produced and propagated in the opposite direction at higher load, 21.8 N, in Fig. 3(c). Finally, immediately after the complete removal of the load, delamination of the TiN film occurs with the shape of a semicircle along the linear defect, as shown in Fig. 3(d). The static indentation response on TiN-coated sapphire corresponded fairly well with the results of the scratch test in the context of failure sequence showing that linear defects were initiated prior to the delamination of the TiN film. In both the scratch tests and the static indentations, the linear defects on the surface of sapphire substrate played a critical role in the failure of TiN coating on sapphire.

To explore the position of linear defects, a series of static indentations were conducted. Figure 4 shows the micrograph of surface damage with top and bottom view of sapphire substrate and TiN film on sapphire after static indentation with a 200-μm diamond cone indenter. The load was applied up to 15, 20, 25 N, respectively. The comparison of micrographs obtained from the top and the bottom view confirmed the position of linear features. The linear defects were not on the surface of TiN film but on the surface of sapphire substrate, as clearly shown in Fig. 4. No linear defect appeared on the surface of TiN film with the top view, which was observed from the surface of TiN film. However, several linear defects appeared with the bottom view, which was observed from the sapphire substrate. Accordingly, the linear defects were produced on the surface of sapphire substrate and the triggered the detachment of TiN film from the sapphire substrate.

To identify the linear defects appearing on the (11$\bar{2}$0) sapphire substrate, the indentation response of a sapphire substrate without TiN coating was investigated with static normal indentations and nanoindentations. Figure 5(a) presents the surface impression after a static indentation using a diamond cone indenter with a tip radius of 200 μm at a maximum load of 20 N. Two distinct two

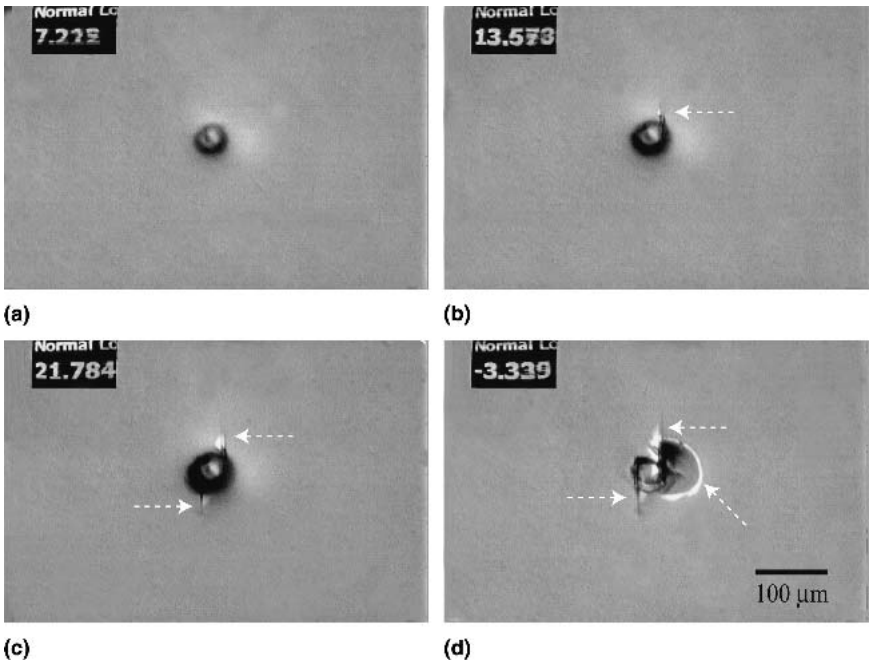

FIG. 3. Sequence of video clips during a static indentation of the same specimen, 700-nm-thick TiN film on sapphire, using a diamond cone indenter with a tip radius of 200 μm.

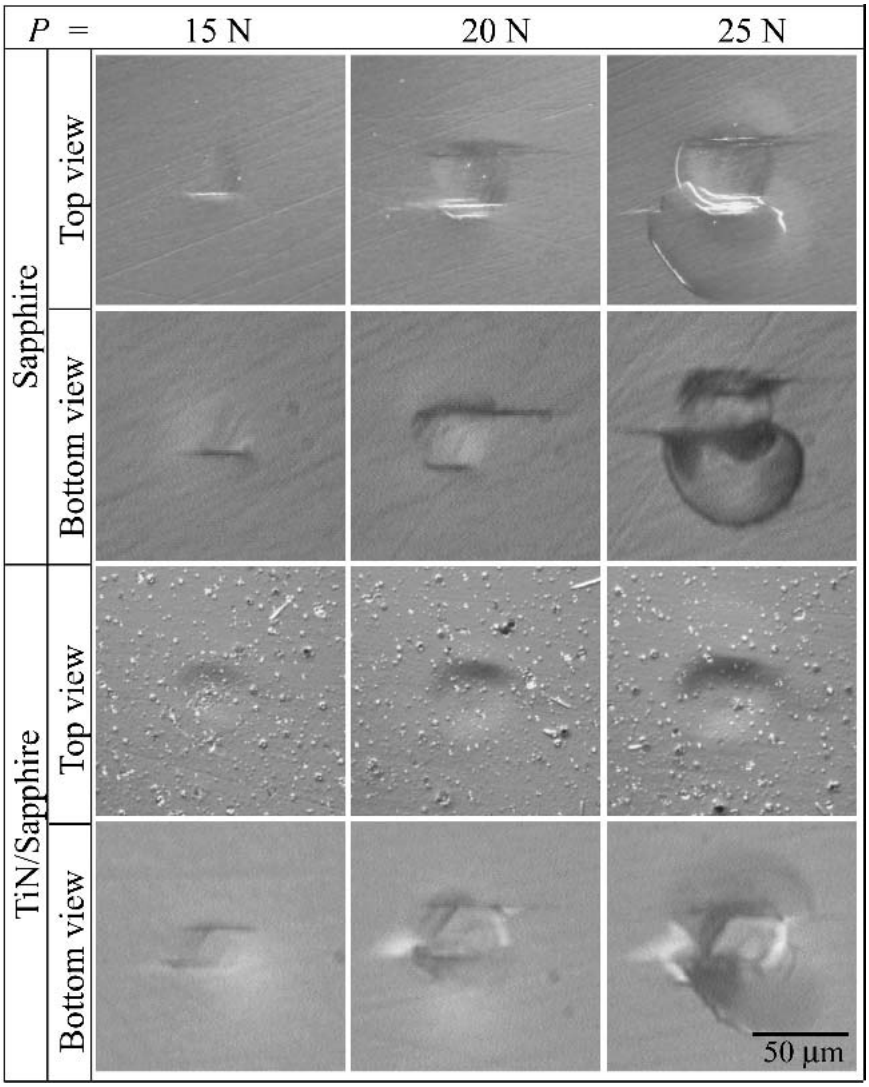

FIG. 4. Micrographs of surface damage with top and bottom view of sapphire substrate and TiN film on sapphire after static indentation with a 200-μm diamond cone indenter. In the case of sapphire, several linear defects were clearly visible on sapphire substrate with top and bottom view after static indentation from 15 N. However, in case of TiN film on sapphire, no linear defect was detected with top view and some linear defects were observed with bottom view. It indicates the linear detect formed on the sapphire substrate.

pairs of parallel linear defects on the sapphire surface are observed. The linear defect looked like a cracking. However, analysis showed the linear features were not cracks but surface traces of deformation twinning of the sapphire substrate. The critical load to induce a twinning is quite low (around 15 N) rather than the critical load to initiate a circumferential (25 N) and a lateral cracking (25 N) of sapphire as shown in Fig. 4. Therefore, the linear feature produced during the previous scratch tests and static indentations are definitely deformation twins of the sapphire. The linear defects on sapphire, so called linear surface features (LSF), have been reported as twin defects.[12–15] Several twin systems in sapphire have been reported.[12,15,16] Rhombohedral and basal twinning were reported to be the most favorable twins in sapphire.[17,18] The linear defects intersected each other at an angle of 122.4°. The crystallographic geometry of the twin planes on the (11$\bar{2}$0) sapphire surface is illustrated in Fig. 4(b) to analyze the angle and the direction of the linear defects. To detect the first linear defect, a series of static indentations with a maximum load of 5, 10, 15, 20, and 25 N were introduced on (11$\bar{2}$0) sapphire. No linear defect was detected up to 10 N, and only one pair of parallel linear defects was initiated and propagated to the A-direction at 15 N, as illustrated in Fig. 5(b). Twins of A-direction were initiated first and then twins of B-direction were produced at higher load. The probability of producing a rhombohedral twin was reported to be slightly higher than that of basal twinning.[17] Therefore, the twins with A-direction were interpreted as rhombohedral twinning and the other twins with B-direction were considered basal twinning. The linear surface features were parallel

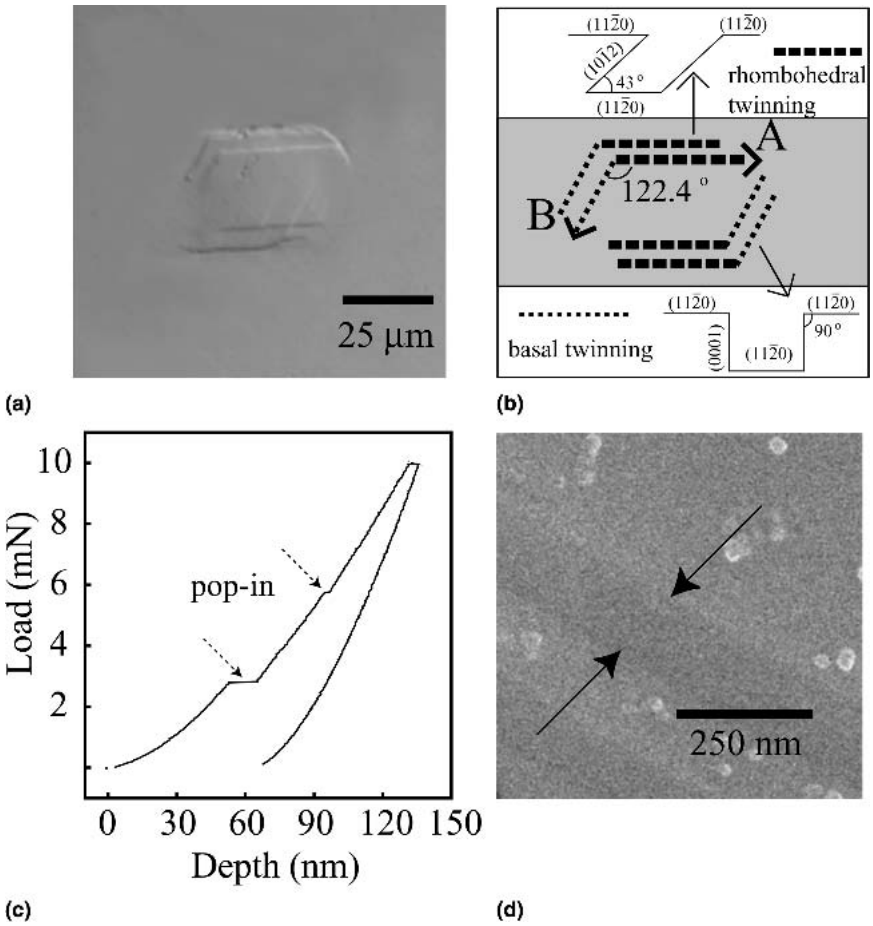

FIG. 5. Identification of twins on (11$\bar{2}$0) sapphire: (a) Linear surface features after a static indentation on the sapphire without TiN film at a maximum load of 20 N. (b) Illustration showing the crystallographic geometry of twin plane projected on the (11$\bar{2}$0) plane of the sapphire. (c) Load–displacement curve during nanoindentation at a maximum load of 10 mN. A peculiar feature known as pop-in was detected in the curve at 2.5 and again at 5.7 mN. (d) SEM micrograph showing one of rhombohedral twins in Fig. 4(a).

to the A-direction, corresponding to the intersection of the rhombohedral plane with the (11$\bar{2}$0) plane of sapphire. The other linear surface features were parallel to the B-direction, corresponding to the intersection of a basal plane with the (11$\bar{2}$0) plane of sapphire. The angle between the rhombohedral and the basal twinning projected on the (11$\bar{2}$0) plane is 122.4°, considering the crystallography of sapphire; this precisely coincided with the angle experimentally observed in Fig. 5(a) In the case of rhombohedral twinning, the (11$\bar{2}$0) plane was inclined at an angle of 43° with the rhombohedral (10$\bar{1}$2) plane. On the other hand, basal twinning was perpendicular to the (11$\bar{2}$0) plane.

The contact-induced response of the sapphire substrate was investigated by nanoindentation with a Berkovich tip of 100-nm curvature. The indentation was carried out in three steps, loading, holding, and unloading. Load was applied up to 10 mN at 200 μN/s, held for 10 s, and then unloaded. Figure 5(c) presents the load–displacement curve during nanoindentation. A peculiar feature known as pop-in was detected in the curve at 2.5 mN and again at 5.7 mN. These pop-in behaviors were induced by cracking or twinning.[15,19] No cracking is observed in Fig. 5(a). Hence, the pop-ins were induced by twins of sapphire, particularly rhombohedral and basal twinning, which are reported as the most favorable twins requiring the lowest resolved shear stress.[19] Accordingly, the linear defects appeared in the scratch test and the static indentation are twins. The twin lamella of rhombohedral twinning can be observed in more detail in the SEM image in Fig. 5(d). One linear line in Fig. 5(a) is composed with several twins and the width of the twin is approximately 180 nm.

In summary, the failure origin of physical vapor deposited TiN film on (11$\bar{2}$0) sapphire was investigated through in situ observations during scratch tests and static indentations. By means of in situ observations, the failure mode of TiN film was clearly demonstrated as linear defects of the sapphire substrate. In PVD TiN film on a (11$\bar{2}$0) sapphire substrate, twinning-induced plastic deformation of the sapphire substrate triggered initiation of interfacial delamination of the TiN coating.

Rhombohedral twinning was initiated first, and basal twinning ensued. Accordingly, plastic deformation of the substrate plays a critical role in determining the fracture of the protective coating.

ACKNOWLEDGMENT

This work was supported by a grant for International Collaboration Research Program from Korea Ministry of Science and Technology (M6-0105-00-0012).

REFERENCES

1. S.V. Hainsworth and W.C. Soh: The effect of the substrate on the mechanical properties of TiN coatings. *Surf. Coat. Technol.* **163–164,** 515 (2003).
2. S. Ma, K. Xu, and J. He: Parametric effects of residual stress in pulsed d.c. plasma enhanced CVD TiN coating. *Surf. Coat. Technol.* **142–144,** 1023 (2001).
3. M.H. Shiao, S.A. Kao, and F.S. Shieu: Effects of processing parameters on the microstructure and hardness of the arc-ion plated TiN on a type 304 stainless steel. *Thin Solid Films* **375,** 163 (2000).
4. B.F. Chen, J. Hwang, G.P. Yu, and J.H. Huang: In situ observation of the cracking behavior of TiN coating on 304 stainless steel subjected to tensile strain. *Thin Solid Films* **352,** 173 (1999).
5. F.S. Shieu, L.H. Cheng, Y.C. Sung, J.H. Huang, and G.P. Yu: Microstructure and coating properties of ion-plated TiN on type 304 stainless steel. *Thin Solid Films* **334,** 125 (1998).
6. M. Larsson, M. Bromark, P. Hedenqvist, and S. Hogmark: Deposition and mechanical properties of multilayered PVD Ti-TiN coatings. *Surf. Coat. Technol.* **76–77,** 202 (1996).
7. H.Z. Durusoy, O. Duyar, A. Aydinli, and F. Ay: Influence of substrate temperature and bias voltage on the optical transmittance of TiN films. *Vacuum* **70,** 21 (2003).
8. V. Talyansky, R.D. Vispute, R. Ramesh, R.P. Sharma, T. Venkatesan, Y.X. Li, L.G. Salamanca-Riba, M.C. Wood, R.T. Lareau, K.A. Jones, and A.A. Iliadis: Fabrication and characterization of epitaxial AlN/TiN bilayers on sapphire. *Thin Solid Films* **323,** 37 (1998).
9. H. Chai, B. Lawn, and S. Wuttiphan: Fracture modes in brittle coatings with large interlayer modulus mismatch. *J. Mater. Res.* **14,** 3805 (1999).
10. R. Saha and W.D. Nix: Effects of the substrate on the determination of thin film mechanical properties by nanoindentation. *Acta Mater.* **50,** 23 (2002).
11. W.C. Oliver and G.M. Pharr: An improved technique for determination hardness and elastic modulus load and displacement sensing indentation experiments. *J. Mater. Res.* **7,** 1564 (1992).
12. M. Wittling, A. Bendavid, P.J. Martin, and M.V. Swain: Influence of thickness and substrate on the hardness and deformation of TiN films. *Thin Solid Films* **270,** 283 (1995).
13. M.V. Swain and M. Wittling: Comparison of acoustic emission from pointed and spherical indentation of TiN films on silicon and sapphire. *Surf. Coat. Technol.* **76–77,** 528 (1995).
14. J.W. Christian and S. Mahajan: Deformation twinning. *Prog. Mater. Sci.* **39,** 1 (1995).
15. R. Nowak, T. Sekino, S. Maruno, and K. Niihara: Deformation of sapphire induced by a spherical indentation on the (10$\bar{1}$0) plane. *Appl. Phys. Lett.* **68,** 1063 (1996).
16. R. Nowak and M. Sakai: The anisotropy of surface deformation of sapphire: Continuous indentation of triangular indenter. *Acta Mater.* **42,** 2879 (1994).
17. R. Nowak, T. Sekino, and K. Niihara: Non-linear surface deformation of the plane of sapphire: Identification of the linear features around spherical impressions. *Acta Mater.* **47,** 4329 (1999).
18. N.I. Tymiak, A. Daugela, T.J. Wyrobek, and O.L. Warren: Acoustic emission monitoring of the earliest stages of contact-induced plasticity in sapphire. *Acta Mater.* **52,** 553 (2004).
19. R. Nowak, C.L. Li, and M.V. Swain: Comparison of implantation with Ni^{2+} and Au^{2+} ions on the indentation response of sapphire. *Mater. Sci. Eng. A* **253,** 167 (1998).